Appl. Phys. A 86, 365–371 (2007)
DOI: 10.1007/s00339-006-3775-x

Applied Physics A
Materials Science & Processing

M.J. ŠĆEPANOVIĆ✉
M. GRUJIĆ-BROJČIN
Z.D. DOHČEVIĆ-MITROVIĆ
Z.V. POPOVIĆ

Temperature dependence of the lowest frequency E_g Raman mode in laser-synthesized anatase TiO_2 nanopowder

Center for Solid State Physics and New Materials, Institute of Physics, Pregrevica 118, 11080 Belgrade, Serbia

Received: 2 August 2006/Accepted: 25 October 2006
Published online: 8 December 2006 •

ABSTRACT Nanosized titanium dioxide (TiO_2) powder was prepared by a laser-induced pyrolysis. Specific surface area of the as-grown powder measured by BET method was 109 m^2/g. The grain size (14.5 nm) estimated from these data coincides well with the crystallite size (12.3 nm) determined by XRD measurements. The average grain size ($\sim$ 35 nm) obtained from the subsequent SEM measurements refers to considerable agglomeration of nanoparticles. Raman spectroscopy has been used to investigate the structural properties of TiO_2 nanopowder and its anatase structure is confirmed. The blueshift and broadening of the lowest frequency E_g Raman mode at temperature range $\sim$ 25–550 K have been analyzed using a phonon-confinement model. Dominant influence of the strong anharmonic effect at higher temperatures was demonstrated.

PACS 81.07.Wx; 78.30.-j; 63.22.+m

1 Introduction

Titanium dioxide (TiO_2) as a highly ionic compound is used in many technical applications such as photovoltaic devices, integrated wave guides, gas and humidity sensors and solar cells. It has been proved to be an excellent catalyst in the photocatalytic degradation of organic pollutants, water/air purifier, and could be widely applied in biomedical and bioengineering fields, due to its strong oxidizing properties, chemical inertness, and nontoxicity [1–3]. Recent interest in nanocrystalline anatase TiO_2 has been driven by its potential in a variety of technological applications, as well as in fundamental studies of size-induced modifications of the physical properties and phase stability of the nanoscale inorganic systems [4, 5]. Raman spectroscopy, a powerful tool in the study of microstructure of nanosized materials, is a promising technique for characterization of TiO_2 nanopowders [6]. The changes in the Raman spectrum of nanocrystalline anatase, the phase most commonly synthesized at ambient conditions, have been variously interpreted as originating from the phonon confinement [7–9], non-stoichiometry [10] or internal stress/surface tension effects [11]. Although the majority of the published studies rested upon phonon confinement as the main factor responsible for the changes observed in the Raman spectrum of nanocrystalline anatase [7–9], some researchers have interpreted their results favoring one of the other factors, depending on structural characteristics of nanopowders. Zhu et al. [12] was the first (and only one, to the best of our knowledge) who presented Raman spectra of anatase TiO_2 nanocrystals (derived from hydrolysis of tetrabutyl titanate) at temperature range 83–293 K and studied the size and temperature dependence of the lowest frequency E_g mode. However, in his paper the calculation using phonon confinement model was based upon strong simplification (such as hypothesis of isotropic dispersion relation) and was carried out only at room temperature, without direct comparison of experimental and calculated spectra. In our paper, a detailed Raman study of anatase TiO_2 nanopowder synthesized by laser-induced pyrolyses with crystallite size about 12.3 nm is presented. Stokes and anti-Stokes Raman spectra at different temperatures in the range from about 25 to 550 K are shown. We demonstrated that the frequency shift and the broadening of the E_g Raman mode are the consequence of the subtle interplay between local heating effects and confinement effects due to the nanocrystalline size, and the influences of these two effects vary with temperature. Applying the phonon confinement model with anisotropic dispersion relations and temperature dependant parameters, we obtain very good agreement between experimental and calculated spectra of anatase TiO_2 nanopowder at all given temperatures.

2 Experimental details

Titanium dioxide nanopowder was synthesized by laser-induced pyrolyses, from vapor phase of $TiCl_4$ and isopropyl alcohol using SF_6 as sensitizer [13, 14]. The produced powder was calcinated in air for 4 h at 500 °C. Specific surface area of as-produced nanopowder was measured by Brunauer–Emmett–Teller (BET) method.

The X-ray diffraction (XRD) measurements were carried out with a Siemens D500/D501 diffractometer using characteristic Cu K_α radiation.

Scanning electron microscopy (SEM) images of the nanopowder were collected using a JOEL-JSM-5300 scanning microscope at 30 kV accelerating voltage. Particle size distribution was determined from program GSD1 developed in our laboratory.

✉ Fax: +381113160531, E-mail: maja@phy.bg.ac.yu

Raman measurements were performed in the backscattering geometry using 514.5-nm line of an Ar^+ laser, Jobin–Yvon U1000 monochromator and the photomultiplier as detector. The measurements at temperatures lower then room temperature were performed in vacuum in the cryostat system. Higher temperatures were achieved by local heating of the sample due to the increasing power (100–700 mW) of laser beam focused by spherical lens. These measurements were performed in air.

3 Material characterization

XRD spectra for TiO_2 nanopowder is shown in Fig. 1. Characteristic diffraction peaks for the anatase phase are present. The average crystallite size, estimated from the main XRD peak (around $2\theta = 25.3°$) using the Sherrer formula, is about 12.3 nm.

Specific surface area of the as-grown powder measured by BET method was 109 m^2/g and the grain size of 14.5 nm was estimated from these data. The agreement between XRD and BET results points out to the possible single crystalline nature of as-grown particles. Alternatively, the greater dimension ($\sim$ 35 nm) of the grains observed by SEM presented in Fig. 2 refers to subsequent agglomeration of nanoparticles.

Raman spectrum at room temperature shown in Fig. 3, confirms the anatase phase of this TiO_2 nanopowder. All observed Raman modes can be assigned to the Raman spectra of the anatase single crystal [15]: $\sim$ 144 cm^{-1} (E_g), 197 cm^{-1} (E_g), 399 cm^{-1} (B_{1g}), 513 cm^{-1} (A_{1g}), 519 cm^{-1} (B_{1g}) and 639 cm^{-1} (E_g). The blueshift and broadening of the lowest frequency anatase E_g Raman mode (at $\sim$ 144 cm^{-1}) at different temperature are particularly analyzed.

4 Results and discussion

The Stokes and anti-Stokes Raman spectra of TiO_2 nanopowder at different temperature are shown in Fig. 4. Lower temperatures ($T < 300$ K) were obtained by the cryostat system in vacuum. Higher temperatures were achieved

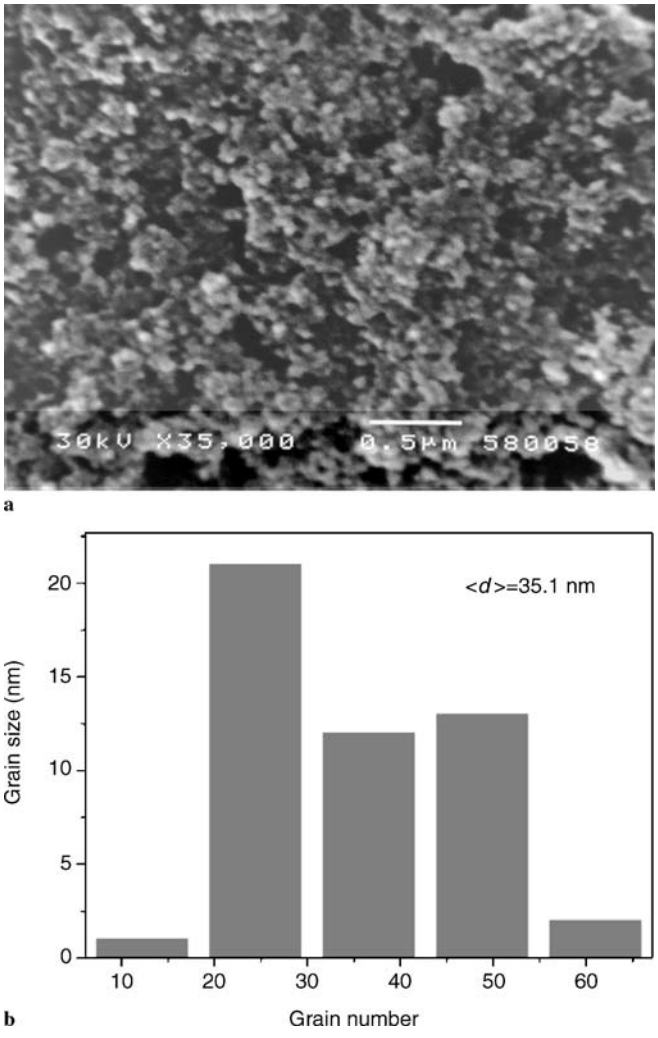

FIGURE 2 SEM micrograph of anatase TiO_2 nanopowder (**a**) and the particle size distribution (**b**)

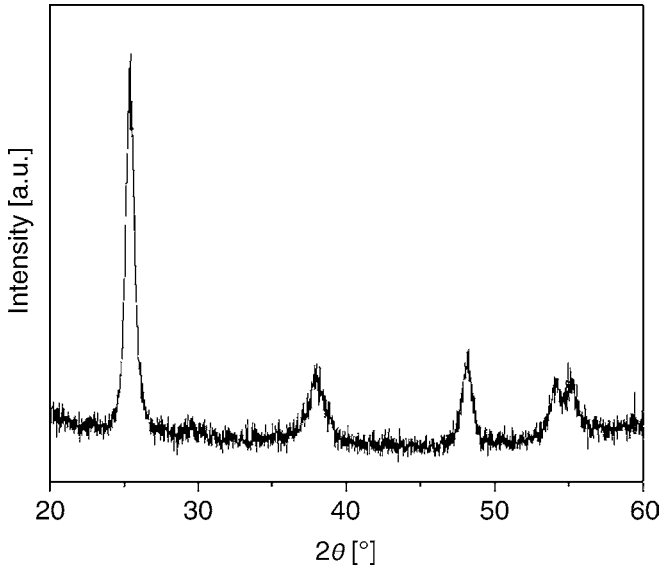

FIGURE 1 XRD spectra of anatase TiO_2 nanopowder

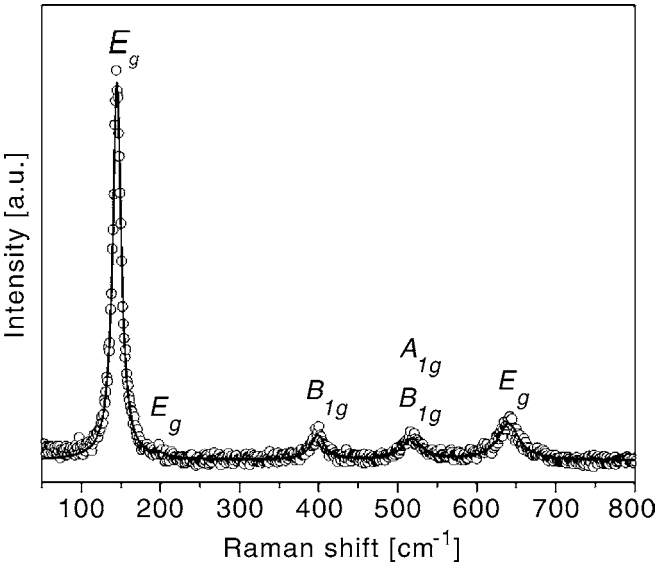

FIGURE 3 Raman spectrum (*open circles*) of anatase TiO_2 nanopowder, fitted on the sum (*thick solid line*) of Lorentzian functions

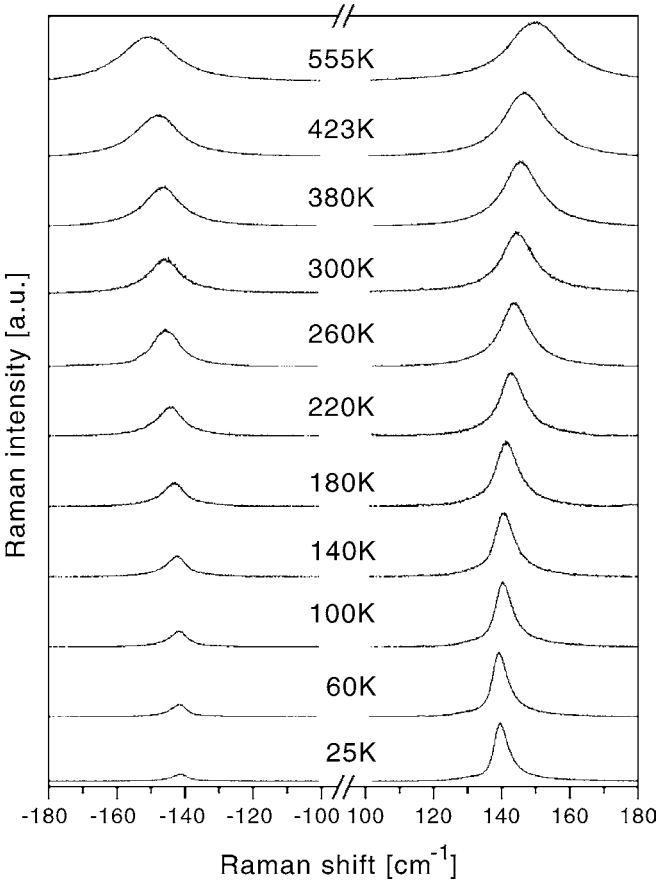

FIGURE 4 The Stokes and anti-Stokes Raman spectra of TiO_2 nanopowder at different temperatures

by local heating of the sample as a consequence of irradiation by focused laser beam with the incident power between 100 and 700 mW. A convenient way to determine the local temperature in the sample is to use the Stokes/anti-Stokes intensity ratio which depends on temperature through the Bose–Einstein occupation number [16]:

$$\frac{I_{\text{Stokes}}}{I_{\text{anti-Stokes}}} = \left(\frac{\omega_L - \omega_s}{\omega_L + \omega_s}\right)^4 \mathrm{e}^{\hbar\omega/k_{\mathrm{B}}T}. \tag{1}$$

We should note that this formula is strictly valid for equilibrium conditions and in the adiabatic limit, which often is not fulfilled in the case of nanomaterials [17]. Also, because of the local heating by laser irradiation, temperatures calculated by (1) are usually higher then ambient temperature measured in cryostat, that is more pronounced at lower temperatures. Therefore using this method of temperature determination, the errors are quite large. Nevertheless, this uncertainty does not influence our main conclusion that the phonon mode hardening and broadening, together with symmetrical line shapes at higher temperatures, is almost entirely the result of the local-heating effects.

Several factors like phonon confinement [6–9, 11, 18, 19], strain [11, 20], non-homogeneity of the size distribution [11, 21], defects and non-stoichiometry [10, 11], as well as anharmonic effects due to temperature increase [12] can contribute to the changes in the peak position, linewidth and shape of the E_g Raman mode in anatase TiO_2 nanopowder. Which of these factors will play an important role in Raman spectra depends on the structural characteristics of the TiO_2 nanopowder: grain size and grain size distribution, existence of mixed phases (anatase in combination of considerable amount of rutile or brookite phase), value and type of the strain (compressed or tensile), discrepancy from the stoichiometry as well as the type of stoichiometric defects, etc.

In the calculation of the Raman intensity of E_g mode, we suppose that the average crystallite size is $L_0 = 12.5$ nm according to XRD measurements. According to the SEM results, we assumed asymmetric Gaussian particle size distribution with the ratio of narrower (at the side of smaller particles, $L < L_0$) to broader (at the side of greater particles, $L > L_0$) half-width of Gaussian of 0.42. The strain value obtained from XRD measurements was relatively small ($\sigma = 0.02\%$), therefore we neglected its influence on E_g mode. Although non-stoichiometry due to laser irradiation in vacuum can cause considerable blueshift and broadening of E_g mode [6, 10, 11], these effects are relatively small in our sample – about 1 cm^{-1}. It seems that the presence of non-stoichiometry defects in this sample preferably induces the appearance of new mode at $\sim 137\ \mathrm{cm}^{-1}$ (at room temperature). This low intensity broad mode can be related to the presence of small amount of nanoparticles of titanium [22]. Note here that the XRD spectrum is not in contradiction with this conclusion as main (002) diffraction peak of titanium at 38° coincides with position of (004) peak of anatase. Also, a small broad feature present at about 29° in spectrum of our sample is observed in titanium films with nanometric thickness [23].

So, phonon confinement and anharmonic effects remain the predominant reasons that affect the shape, shift and linewidth of E_g mode, and we try to resolve the influence of both these effects in further analyses. The asymmetrical shape of the E_g mode at low temperature originates mainly from phonon confinement, while symmetrical shape of this mode at higher temperatures points out to the greater influence of anharmonic effects. The estimation of these influences has been performed in detail and its results will be presented below.

The phonons in nanocrystal are confined in space and all the phonons over the entire Brillouin zone will contribute to the first-order Raman spectra. The weight of the off-center phonons increases as the crystal size decreases and the phonon dispersion causes an asymmetrical broadening and the shift of the Raman mode. According to the phenomenological work of Richter et al. [18] and Campbell et al. [19] for spherical particle of diameter L and Gaussian confinement function, the resulting Raman intensity $I(\omega)$ can be presented as a superposition of weighted Lorentzian contributions over the whole Brillouin zone [17, 19]

$$I(\omega) = \sum_{i=1}^{m} \int_0^{\infty} \varrho(L)\mathrm{d}L \int_{\mathrm{BZ}} \frac{\exp\left(\frac{-q^2L^2}{8\beta}\right)\mathrm{d}^3q}{[\omega - \omega_i(q,T)]^2 + \left(\frac{\Gamma(T)}{2}\right)^2}, \tag{2}$$

where $\varrho(L)$ is the particle size distribution, q is wave vector expressed in units of π divided by value of unit cell parameter, and $\Gamma(T)$ is the mode line width at temperature T. The sum is carried over m dispersion curves $\omega_i(q, T)$, depending on mode degeneration. The factor β varies from $\beta = 1$ in the Richter

confinement model to $\beta = 2\pi^2$ in the Campbell model depending on the confinement boundary conditions in different nanomaterials. The properties of Raman mode simulated by this model strongly depend on the values of mean particle size and unit cell parameter, as well as the choice of the values of $\Gamma(T)$, and β. Also, the particle size distribution $\varrho(L)$ and the shape of the phonon dispersion relations $\omega_i(q)$ has a large influence on the position and asymmetry of the calculated spectra. Sometimes different combination of these choices can give similar results. For instance, the application of strong confinement condition, i.e., great β parameter, in combination with phonon dispersion curve with small slope [8, 24] can give similar calculation results for E_g Raman mode in anatase TiO_2 nanocrystals as the weaker confinement and dispersion curve with greater slope [6, 12].

Several groups have tried to apply the phonon confinement model in order to find a correlation between the shift and width of the E_g anatase mode at $\sim 144\,\mathrm{cm}^{-1}$ and the crystalline domain size [6, 8, 9, 24, 25]. Unfortunately, published results are sometimes confusing and often contradictory. The main problem when using this model is the lack of experimental dispersion relations of anatase TiO_2 from inelastic neutron scattering. Anatase phonon dispersion relations have been computed by Mikami et al. [26] using density-functional theory techniques. According to these theoretical curves of anatase, the dispersion relations in this paper are approximately expressed in the cosine form [12]

$$\omega_i(q, T) = \omega_0(T) + B_i\,(1 - \cos(q\pi))\ , \qquad (3)$$

where $\omega_0(T)$ is frequency of the E_g mode in Γ point at temperature T. The values of B_i constants are calculated to match the phonon dispersion curves, depending on direction throughout Brillouin zone. We assumed $B_1 = 102\,\mathrm{cm}^{-1}$ and $B_2 = 28\,\mathrm{cm}^{-1}$ in Γ-X direction, $B_3 = 52\,\mathrm{cm}^{-1}$ and $B_4 = 15\,\mathrm{cm}^{-1}$ in Γ-N direction, and $B_5 = 18\,\mathrm{cm}^{-1}$ in Γ-Z direction. Those curves are presented in the inset of Fig. 5a.

The angular integral in a wave vector space in the Brillouin zone is performed by integrating along the Γ-X, Γ-N, and Γ-Z symmetry directions, weighting each by the number of equivalent symmetry directions. The weighted mode intensities calculated according to the relation (2) at room temperature for different dispersion curves (a–e) are shown separately in Fig. 5a. The integrated contributions along three directions mentioned above are shown in Fig. 5b. From this figure, it can be seen that the contribution along all directions have similar shape and position. This may be an explanation why the approximation of isotropic dispersion relations applied in earlier works [4–9] had given good results. Here we assumed factor $\beta \approx 16$. The values of $\omega_0(T)$, as well as those of $\Gamma(T)$, at specified temperature were treated as adjusting parameters in the fitting procedure and were listed in Table 1. The comparison of the normalized experimental and calculated spectra according to described procedure at several temperatures are shown in Fig. 6. The position, width and relative integrated intensity (when the intensity of E_g mode is normalized) of additional mode attributed to titanium are shown in Table 2 for different temperatures. The maximum relative intensity of this mode is obtained at 260 K, as it could be expected regarding the greatest non-stoichiometry due to the laser irradiation in vacuum at this temperature. Also, intensity of this mode decreases with temperature increase, as non-stoichiometry decreases due to powerful laser irradiation in air.

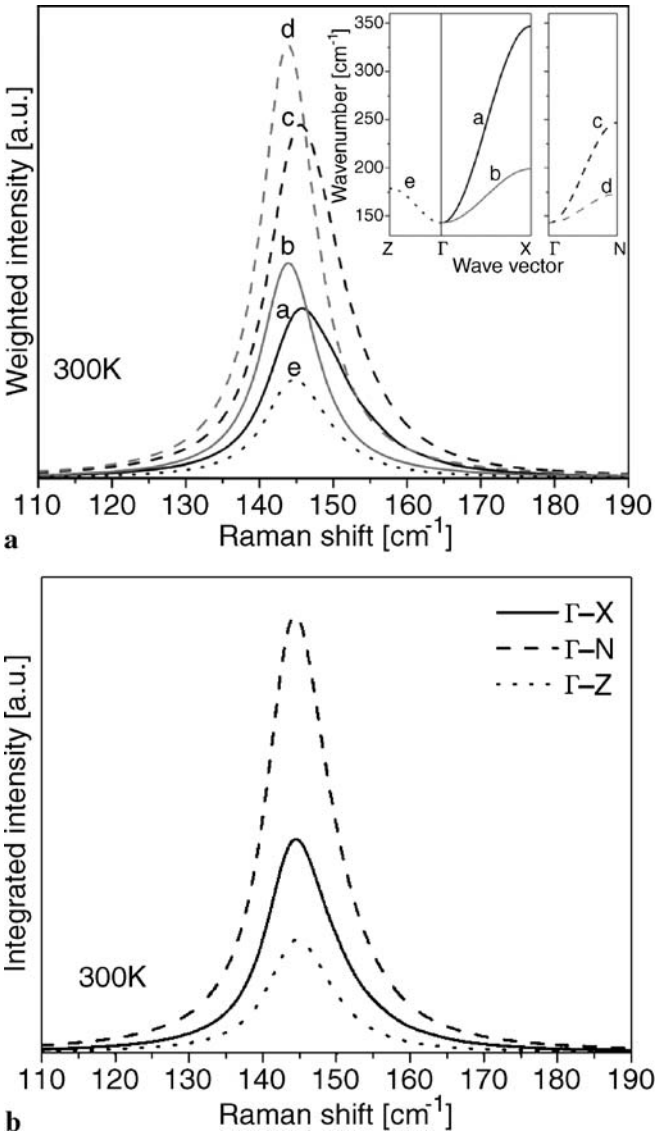

FIGURE 5 The weighted mode intensities (see the text) calculated at room temperature with corresponding phonon dispersion curves in the *inset* (**a**) and the integrated contributions along Γ-X, Γ-N and Γ-Z directions of Brillouin zone (**b**)

T[K]	$\Gamma(T)$ [cm^{-1}]	$\omega_0(T)$ [cm^{-1}]
25	3.0	138.3
60	3.5	138.5
100	4.3	139.0
140	5.0	139.5
180	5.5	140.2
220	6.3	141.2
260	7.6	142.0
300	8.5	142.8
380	11.5	144.1
423	13.5	145.2
555	18.0	147.7

TABLE 1 The temperature dependence of adjusting parameters $\omega_0(T)$ and $\Gamma(T)$ applied in simulation of E_g mode

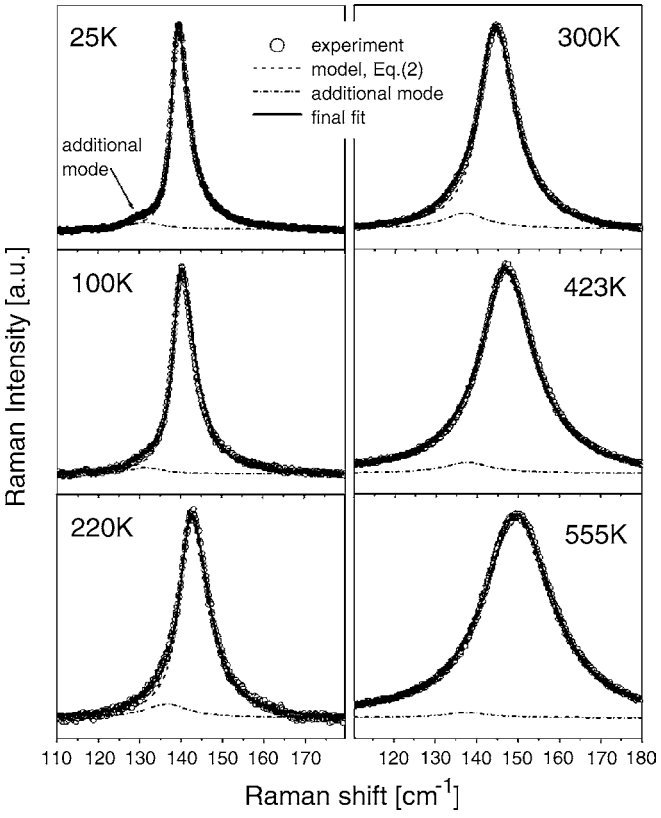

FIGURE 6 The normalized experimental (*open circles*) and calculated (*solid lines*) spectra of anatase TiO_2 nanopowder

T[K]	ω_a[cm^{-1}]	w_a[cm^{-1}]	Relative intensity
25	131.5	10	0.5
60	131.5	10	0.5
100	131.5	10	0.5
140	132.5	10	0.7
180	134.5	11	0.9
220	136.5	13	1.4
260	136.5	13	2.0
300	136.5	13	1.6
380	137.5	13	1.5
423	137.5	15	1.0
555	137.5	15	0.6

TABLE 2 The position (ω_a), linewidth (w_a) and intensity of additional Raman mode attributed to titanium at different temperatures

As we have already mentioned, our Raman spectra show that the phonon line shapes are approximately symmetric regardless of the frequency shifts and the broadening at higher temperatures. Thus, in the following part of the paper, we describe the influence of anharmonic effects on the Raman spectra. Anharmonicity is incorporated through the three- and four-phonon decay channels in the scattering process [20, 27]:

$$\omega(q,T) = \omega_0(q) + \Delta(T)\,, \tag{4}$$

$$\Delta(T) = A_1\left[1+\sum_{j=1}^{2}\frac{1}{\exp(x_j)-1}\right] + A_2\left[1+\sum_{k=1}^{3}\frac{1}{\exp(y_k)-1}+\frac{1}{(\exp(y_k)-1)^2}\right], \tag{5}$$

$$\Gamma(T) = \Gamma_0 + \Delta\Gamma(T)\,, \tag{6}$$

$$\Delta\Gamma(T) = B_1\left[1+\sum_{j=1}^{2}\frac{1}{\exp(x_j)-1}\right] + B_2\left[1+\sum_{k=1}^{3}\frac{1}{\exp(y_k)-1}+\frac{1}{(\exp(y_k)-1)^2}\right]. \tag{7}$$

The first terms in (5) and (7) describe the coupling of the optical phonon to two lower-energy phonons (three-phonon coupling, with $x_1 = x_2 = h\omega_0/2kT$) which is $\propto T$ at higher temperatures, and the second terms describe the coupling to three phonons (four-phonon coupling, with $y_1 = y_2 = h\omega_0/3kT$) which is $\propto T^2$ at higher temperatures.

Experimental dependence of the peak position and width on measured (solid symbols) and calculated (open symbols) temperature for our sample is presented in Fig. 7a and b, respectively. The data calculated using the relations for anharmonic effects with neglected third term in (5) and (7) are shown in the same figures by full lines. The values of anharmonic parameters (in cm^{-1}) are assumed as those for TiO_2 nanopowder with grain size of 12.7 nm from [12]: $\omega_0(q) = 137.5$, $A_1 = 1.18$, $\Gamma_0 = 2.62$, $B_1 = 1.52$, $A_2 = 0$ and $B_2 = 0$. The agreement between experimental and calculated data is optimal in the temperature region between 100 and 300 K, that was expected as in this region the error in determination of temperature is the smallest.

In the Fig. 8a and b the calculated contribution of confinement and anharmonic effects to the shift and linewidth of E_g mode at different temperatures are presented separately. As expected, these contributions are comparable at low temperatures, while the contribution due to anharmonic effect at high temperatures far exceeds contribution of confinement effect. Besides, the part of the blueshift originated from phonon confinement has similar values (about 1.8 cm^{-1}) at all temperatures, while the contribution of confinement to the broadening of E_g mode varies with temperature. The greatest broadening due to confinement at 260 K may be a consequence of additional linewidth increase due to non-stoichiometry induced by laser irradiation in vacuum. On the other side, a decrease of such broadening with temperature increase may be induced by very large mode linewidth $\Gamma(T)$ at high temperatures. Note that the small part (about 1 cm^{-1}) of the line broadening attributed here to the anharmonic effect could originate from the other types of broadening that do not depend on thermal population of phonons, such as instrumental and/or intrinsic broadening (due non-stoichiometry here) [20].

Finally, we can conclude that neglecting the influence of anharmonic effect on E_g Raman mode even at room temperature leads to great inaccuracy in application of phonon confinement model and determination of corresponding parameters in case of TiO_2 nanopowders. Also it could be the reason of discrepancies between experimental data and simulation spectra, especially on the low-frequency side of E_g mode, in earlier works [6, 12, 24]. Of course, knowledge of the exact form of dispersion relations for TiO_2 nanopowder at different temperatures should be known in order to perform the exact computation and determin-

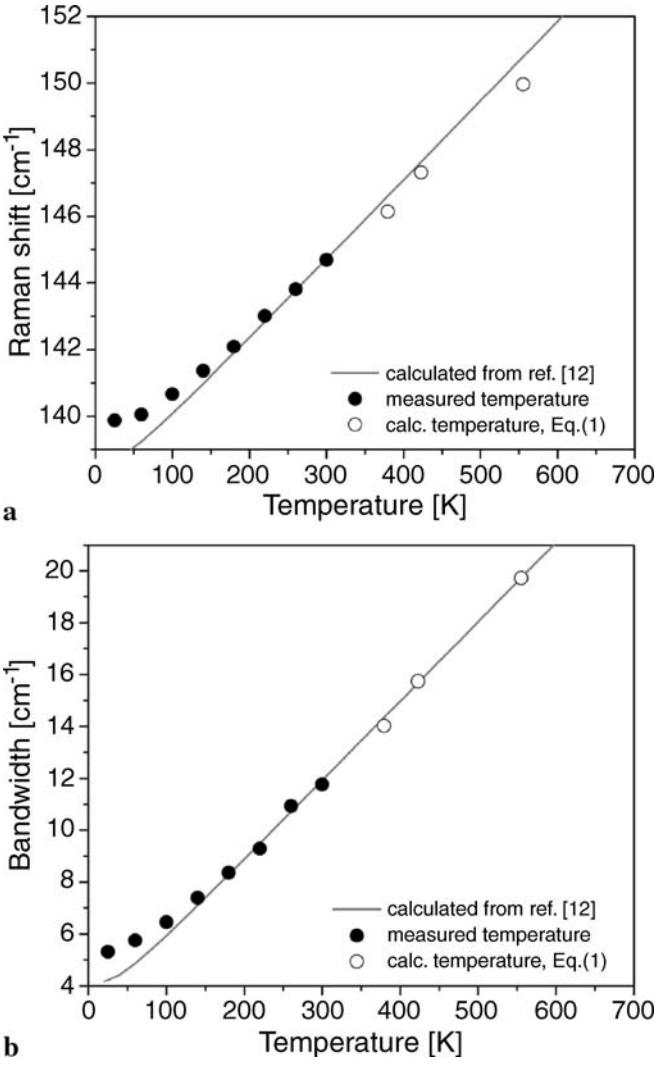

FIGURE 7 The experimental dependence of the E_g peak position (**a**) and linewidth (**b**) on measured (*solid circles*) and calculated (*open circles*) temperature in comparison with the corresponding data calculated by the anharmonic relations [12] (*solid lines*)

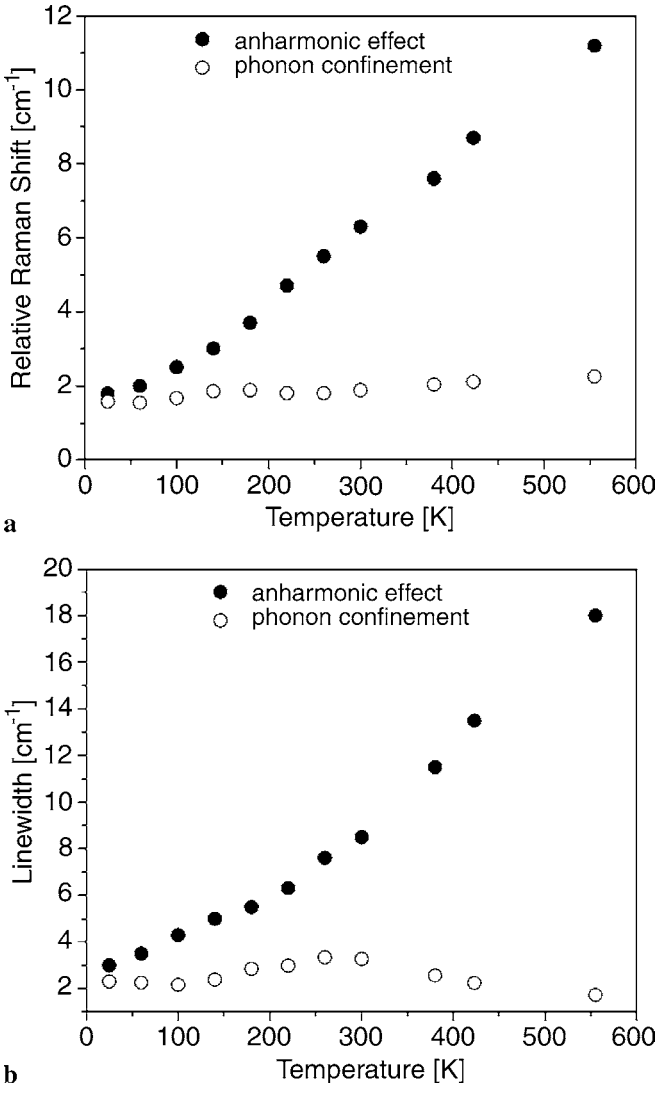

FIGURE 8 The calculated contribution of confinement (*open circles*) and anharmonic (*solid circles*) effects to the shift (**a**) and linewidth (**b**) of E_g mode at different temperatures

ation of the parameters included in the phonon confinement model.

5 Conclusion

We have performed a systematic characterization of TiO_2 nanopowder produced by laser-induced pyrolysis. In order to assess the reliability of the Raman spectroscopy as an efficient technique for the characterization of the TiO_2 nanopowders, we have investigated the behavior of the E_g Raman mode of anatase TiO_2 at different temperatures. Among several factors affecting the shape, shift and linewidth of this mode (such as strain, non-homogeneity of the size distribution, defects and non-stoichiometry) depending of the type of TiO_2 nanopowders, we have concluded that the phonon confinement and anharmonic effects were the effects with the greatest contribution. Application of the phonon confinement model including anisotropic dispersion relations with temperature dependant parameters has produced very good agreement between experimental and simulated E_g Raman mode at all given temperatures. These results have shown that the contributions of confinement and anharmonic effects are comparable at low temperatures, while the contribution due to anharmonic effect at high temperatures far exceeds contribution of confinement effect.

ACKNOWLEDGEMENTS This work was supported by the Serbian MSEP under the project No.141 047. We would like to express our thanks to Dr B. Matović who provided XRD data.

REFERENCES

1 P.A. Christensen, T.P. Curtis, T.A. Egerton, S.A.M. Kosa, J.R. Tinlin, Appl. Catal. B **41**, 371 (2003)
2 S.S. Hong, M.S. Lee, H.S. Hwang, K.T. Lim, S.S. Park, C.S. Ju, G.D. Lee, Sol. Energ. Mater. Sol. C **80**, 273 (2003)
3 B. Miller, E. Pujads, E. Gocke, Environ. Mol. Mutagen. **26**, 240 (1995)
4 V. Swamy, A. Kuznetsov, L.S. Dubrovinsky, R.A. Caruso, D.G. Shchukin, B.C. Muddle, Phys. Rev. B **71**, 184 302 (2005)
5 H. Zhang, J.F. Banfield, J. Mater. Chem. **8**, 2073 (1998)
6 A. Li Bassi, D. Cattaneo, V. Russo, C.E. Bottani, E. Barborini, T. Mazza, P. Piseri, P. Milani, F.O. Emst, K. Wegner, S.E. Pratsinis, J. Appl. Phys. **98**, 074 305 (2005)

7 S. Kelly, F.H. Pollak, M. Tomkiewicz, J. Phys. Chem. B **101**, 2730 (1997)
8 D. Bersani, P.P. Lottici, Appl. Phys. Lett. **72**, 73 (1998)
9 W.F. Zhang, Y.L. He, M.S. Zhang, Z. Yin, Q. Chen, J. Phys. D Appl. Phys. **33**, 912 (2000)
10 J.C. Parker, R.W. Siegel, Appl. Phys. Lett. **57**, 943 (1990)
11 M.J. Šćepanović, M.U. Grujić-Brojčin, Z.D. Dohčević-Mitrović, Z.V. Popović, Mater. Sci. Forum **518**, 101 (2006)
12 K.R. Zhu, M.S. Zhang, Q. Chen, Z. Yin, Phys. Lett. A **340**, 220 (2005)
13 F. Curcio, M. Musci, N. Notaro, C. Nannetti, Appl. Surf. Sci. **36**, 52 (1989)
14 F. Curcio, M. Musci, N. Notaro, G. De Michele, Appl. Surf. Sci. **46**, 225 (1990)
15 T. Ohsaka, F. Izumi, Y. Fujiki, J. Raman Spectrosc. **7**, 321 (1978)
16 P. Brüesch, *Phonons: Theory and Experiments II* (Springer, Berlin, 1986)
17 M.J. Konstantinović, S. Bersier, X. Wang, M. Hayne, P. Lievens, R.E. Silverans, V.V. Moshchalkov, Phys. Rev. B **66**, 161 311 (2002)
18 H. Richter, Z.P. Wang, L. Ley, Solid State Commun. **39**, 625 (1981)
19 I.H. Campbell, P.M. Fauchet, Solid State Commun. **58**, 739 (1984)
20 J.E. Spanier, R.D. Robinson, F. Zhang, S.W. Chan, I.P. Herman, Phys. Rev. B **64**, 245 407 (2001)
21 D.R. Santos, I.L. Torriani, Solid State Commun. **85**, 307 (1993)
22 J. Nemanich, C.C. Tsai, G.A.N. Connell, Phys. Rev. Lett. **44**, 273 (1980)
23 K. Cai, M. Müller, J. Bossert, A. Rechtenbach, K.D. Jandt, Appl. Surf. Sci. **250**, 252 (2005)
24 M. Ivanda, S. Musić, M. Gotić, A. Turković, A.M. Tonejc, O. Gamulin, J. Mol. Struc. **480**, 641 (1999)
25 A. Pottier, S. Cassaignon, C. Chaneac, F. Villain, E. Tronc, J.P. Jolivet, J. Mater. Chem. **13**, 877 (2003)
26 M. Mikami, S. Nakamura, O. Kitao, H. Arakawa, Phys. Rev. B **66**, 155 213 (2002)
27 M. Balkanski, R.F. Wallis, E. Haro, Phys. Rev. B **28**, 1928 (1983)